NUCL SCI TECH (2021) 32:96
https://doi.org/10.1007/s41365-021-00933-8

Yield of long-lived fission product transmutation using proton-, deuteron-, and alpha particle-induced spallation

Meng-Ting Jin[1] · Su-Yang Xu[1] · Guan-Ming Yang[1] · Jun Su[1]

Received: 21 January 2021 / Revised: 30 July 2021 / Accepted: 31 July 2021 / Published online: 8 September 2021

Abstract The transmutation of long-lived fission products through spallation induced by light nuclides was investigated for the purpose of determining the feasibility of this approach for long-lived fission products, in both economic and environmental terms. The cross-section data were obtained from the TALYS Evaluated Nuclear Data Library (TENDL). A thick target model was used to study the consumption of the target isotopes in the transmutation process. The transmutation yield was calculated using the highest beam intensity available with the China initiative accelerator-driven system. It was found that the light nuclide-induced spallation reaction can significantly reduce the radio toxicity of the investigated long-lived fission products. Using the transmutation target made of elemental LLFP and the proton beam with an intensity of 5 mA, the consumption of ^{90}Sr, ^{93}Zr, ^{107}Pd, or ^{137}Cs can reach approximately 500 g per year.

Keywords Transmutation · Long-lived fission products · Spallation

This work was supported by the National Natural Science Foundation of China (No. 11875328).

✉ Jun Su
sujun3@mail.sysu.edu.cn

1 Sino-French Institute for Nuclear Energy and Technology, Sun Yat-sen University, Zhuhai 519082, China

1 Introduction

Nuclear power is considered as an essential part of national energy systems in many countries because it is economically competitive and plays an important role in carbon emission reduction [1–4]. Today, however, nuclear power is still wrestling with public acceptance [5]. Some of the opposition arises from the long-lived radioactive waste produced during the operation of nuclear reactors [6, 7]. To meet the requirements of the radiologically clean nuclear power concept, the use of neutrons and a set of quantitative criteria have been proposed for the transmutation of long-lived radioactive waste [8]. The concept of transmutation can be defined as the transformation of one isotope into another isotope using nuclear reactions [9]. In recent decades, there has been increasing interest in accelerator-driven system (ADS) for the transmutation of nuclear waste due to the distrust of deep burial and opposition to the construction of disposal sites [5, 10].

High-level radioactive waste has two main components: long-lived fission products (LLFP) and minor actinides [11]. The development and quantity of the research on the transmutation of these two components are not balanced, as noted in a report of IAEA published in 2004 [12]. The transmutation of minor actinides by neutron irradiation using an ADS has been studied in detail for reprocessing spent nuclear fuel [13–16]. In contrast, research on LLFP transmutation is not sufficiently extensive, although experimental and theoretical works can be found in the literature [17]. The LLFP will be generated continuously in nuclear reactors and ADSs without being consumed in the next generation of nuclear reactors, as they are not considered to be useful materials for power generation [11]. In addition, it has been noted that LLFP may contribute to the radiotoxicity and radiation dose risk from spent fuel in geological disposal [18]. Thus, more attention may be taken to exploit the transmutation of LLFP.

So far, studies on transmutation reactions have focused on neutron-induced nuclear reactions. However, it has been noted that the transmutation of LLFP is a purely neutron-consuming process and requires excess neutrons [19]. Therefore, obtaining neutrons whose energy and beam intensity satisfy the demands of transmutation has become the primary issue [18]. In addition to the possibility of generating excess neutrons in light water reactors or fast reactors, the use of ADS or fusion-driven transmuter to generate the excess neutrons required for the transmuter has also been extensively studied [19–21]. The China Spallation Neutron Source (CSNS), completed in March 2018, was the first spallation neutron source built in China. Based on this facility and its extended research platforms, a great number of studies on nuclear reactions induced by neutrons, especially high-energy neutrons, have been carried out [22–24].

To reduce the quantity of LLFP, transmutation using photodisintegration reactions with bremsstrahlung γ-rays or laser Compton scattering γ-rays has been investigated over recent decades [25–28]. Harada et al. have proposed performing transmutation by using charged particles with energy higher than 100 MeV [29]. The advantages of charged particle transmutation over neutron-induced reactions in terms of economic effects, nuclear risks, and public acceptability are described in Refs. [17, 30]. One problem with transmuting cesium with neutrons is the formation of ^{135}Cs through the double thermal neutron caption of ^{133}Cs without isotopic separation. However, ^{137}Cs and ^{135}Cs are transformed into stable Ba through the (p,n) reaction [30]. Another problem with neutron-induced transmutation for LLFP is that ^{137}Cs and ^{190}Sr, as two main components of LLFP (40% weight fraction), have small thermal neutron-capture cross sections [17, 31, 32].

Experimental work measuring the cross-section data can be found in recent publications, such as Ref. [17]. In addition, evaluated cross sections have been obtained and compiled into nuclear data libraries. One example is the JENDL/ImPACT-2018, which contains the neutron and proton cross sections of 163 nuclides, including four typical long-lived fission products, ^{79}Se, ^{93}Zr, ^{107}Pd, and ^{135}Cs, with an energy range of up to 200 MeV [33]. Another example is the TENDL, which can provide a larger energy range from 1 MeV to 200 MeV for neutron-, proton-, deuteron-, and alpha particle-induced spallation reactions with LLFP. Bayesian neural network (BNN) methods were used to predict the cross sections of residue fragments in proton-induced spallation reactions in a recent study [34]. In addition, efforts have been made to contribute to the prediction of the cross sections for deuteron-induced spallation of long-lived fission products with the IQMD+GEMINI model, and to the understanding of reaction mechanics [35–37].

However, except for the measurement and evaluation of charged particle-induced reaction cross sections of LLFP, the influence of the charge interaction on transmutation performance has not been thoroughly investigated, neither for long-lived isotopes nor for other radioisotopes that can be newly produced in the transmutation process.

In the scientific literature concerning the transmutation of LLFP, ^{90}Sr ($T_{1/2}$ = 29 y), ^{137}Cs ($T_{1/2}$ = 30 y), ^{107}Pd ($T_{1/2}$ = 6.5$\times$10^6 y), and ^{93}Zr ($T_{1/2}$ = 1.61$\times$10^6 y) have received significant attention. ^{90}Sr and ^{137}Cs have a large weight fraction in LLFP and significant radiotoxicities in the first 100 years after reprocessing spent fuel [17]. ^{107}Pd and ^{93}Zr easily diffuse in deep burial processing because of their extremely long half-lives [25]. Thus, the transmutation of these four isotopes is investigated in this work.

The purpose of this study is to investigate the feasibility of transmuting the LLFP ^{90}Sr, ^{93}Zr, ^{107}Pd, and ^{137}Cs with neutrons, protons, deuterons, or α particles under the highest beam irradiation of charged particles currently available, such as in the China initiative accelerator-driven system (CiADS) [38, 39]. The remainder of this paper is organized as follows. In Sect. 2, we briefly describe the proposed method. In Sect. 3, we present the results and discussion. Finally, a summary is provided in Sect. 4.

2 Method

To study the transmutation performance of ^{90}Sr, ^{137}Cs, ^{107}Pd, and ^{93}Zr through light nuclide-induced spallation, a thick target model was adopted. In this model, a thick target is considered. It is assumed that the target is sufficiently thick and covered with a beryllium layer to prevent the leakage of neutrons.

Assume that a beam with intensity I and energy E hits a target of nucleus density N and thickness dx. The number of target nuclei consumed by nuclear reactions per unit time and area dn is given by the definition of the nuclear cross section as

$$\mathrm{d}n = -IN\sigma \mathrm{d}x. \tag{1}$$

Because σ is in [cm^2], dx is in [cm], and N is in [cm^{-3}], dn has the same dimension as I.

The nucleus density of the target N is given by

$$N = \frac{\rho N_{\mathrm{A}}}{M_{\mathrm{t}}}, \tag{2}$$

where $M_{\rm t}$ is the molar mass of the target material given in $[\mathrm{g \cdot mol^{-1}}]$, ρ is the density of the target nuclei given in $[\mathrm{g \cdot cm^{-3}}]$, and $N_{\rm A}$ is the Avogadro constant.

It is assumed that the target has a thickness larger than the range of the incident particles. Thus, an incident particle would not travel through the target before stopping in the absorber material, and the yield of transmutation Y is given by

$$Y = \int_0^n \frac{\mathrm{d}n}{I} = \int_0^R \sigma \frac{\rho N_{\rm A}}{M_{\rm t}} \mathrm{d}x, \tag{3}$$

where R is the range of the incident particle. Y is dimensionless and represents the percentage of incident particles that induce transmutation of LLFP.

To replace the integral with respect to the thickness with an integral with respect to the particle energy, the specific energy loss S for charged particles in the absorber is introduced as a function of beam energy E and given by

$$S(E) = -\frac{\mathrm{d}E}{\mathrm{d}x}. \tag{4}$$

Because the cross-section σ and the specific energy loss S are functions of the particle energy, and the other physical quantities shown in Eqs.(3) and (4) are independent of the energy, it is deduced that

$$Y = \int_0^{E_0} \sigma(E) \frac{\rho N_{\rm A}}{M_{\rm t}} \frac{1}{S(E)} \mathrm{d}E, \tag{5}$$

where E_0 is the incident energy.

For a projectile with kinetic energy E, charge number z, atomic number A, and mass m traveling a distance x into a target of electron number density n_0 given in $[\mathrm{cm^{-3}}]$ and mean excitation and ionization potential P, the specific energy loss S is given in $\mathrm{MeV \cdot cm^{-1}}$ by the Bethe formula as

$$S(E) = \frac{4\pi z^2 n_0}{m_0 \beta^2 c^2} \left(\frac{e^2}{4\pi\varepsilon_0}\right)^2 \left[\ln\frac{2m_0\beta^2c^2}{P} - \ln\left(1-\beta^2\right) - \beta^2\right], \tag{6}$$

where c is the speed of light in a vacuum, m_0 is the electron rest mass, and e is the electron charge [40].

The quantity β^2 is a function of the projectile kinetic energy E, and is given by

$$\beta^2 = 1 - \left(\frac{mc^2}{E + mc^2}\right)^2, \tag{7}$$

where E is in [eV].

For an isotope with atomic number A, the particle mass m is calculated as follows:

$$m = A \cdot amu. \tag{8}$$

For the spallation target made of a single element with atom number Z and nucleus density N, the electron number density n_0 is calculated as follows:

$$n_0 = ZN = \frac{\rho N_{\rm A} Z}{M_{\rm t}}. \tag{9}$$

For the spallation target made of a compound, the electron number density n_0 is calculated as follows:

$$n_0 = Z_{\rm C} N_{\rm C}, \tag{10}$$

where $Z_{\rm C}$ and $N_{\rm C}$ are the charge number and nucleus density of the compound, respectively.

For a compound $\mathrm{B}_x\mathrm{D}_y$, the charge number $Z_{\rm C}$ is given by

$$Z_{\rm C} = xZ_{\rm B} + yZ_{\rm D}, \tag{11}$$

and the nucleus density is given by

$$N_{\rm C} = \frac{\rho_{\rm C} N_{\rm A}}{M_{\rm C}} = \frac{\rho_{\rm C} N_{\rm A}}{xA_{\rm B} + yA_{\rm D}} \tag{12}$$

where $\rho_{\rm C}$ is the density of the compound, $A_{\rm B}$ is the atom number of isotope B, and $A_{\rm D}$ is the atom number of isotope D.

Reference [41] indicates that for a spallation target made of a single element with atomic number Z, the mean excitation and ionization potential P is given by Eq. (6) in eV as

$$P = \begin{cases} 13Z(\mathrm{eV}) \\ 9.76Z + 58.8Z^{-0.19}(\mathrm{eV}) \end{cases} \tag{13}$$

For the spallation target made of the compound $\mathrm{B}_x\mathrm{D}_y$, the mean excitation and ionization potential of the compound P is estimated as

$$P = \frac{xP_{\rm B} + yP_{\rm D}}{x + y}, \tag{14}$$

where $P_{\rm B}$ and $P_{\rm D}$ are the ionization potentials of isotopes B and D, respectively, which can be calculated using Eq. (13).

The constants used in this work are $\frac{e^2}{4\pi\varepsilon_0} = 1.4399 \times 10^{-13}$ MeV $\cdot$ cm, $m_0 = 511000$ eV $\cdot\, \mathrm{c}^{-2}$, and $amu = 931.5$ MeV.

It should be noted that only the nuclear reaction between the incident particles and the LLFP is taken into consideration when calculating the yield of transmutation Y for the spallation target made of compounds.

In this work, the thick target model is adopted to calculate the yield of transmutation Y in the transmutation process of ^{90}Sr, ^{137}Cs, ^{107}Pd, and ^{93}Zr. The proton-, deuteron-, and α particle-induced spallation reactions were studied and compared with the neutron-induced spallation reaction with respect to the consumption of target nuclei.

The calculation of these spallation systems relies on the input of cross-section data over a large energy range. Because of the lack of experimental data on the charged particle-induced spallation reaction of ^{90}Sr, ^{137}Cs, ^{107}Pd, and ^{93}Zr, the input cross-section data were taken from TENDL-2015.

3 Results and discussions

3.1 Spallation production cross section

To evaluate the ability of protons, neutrons, deuterons, and α particles to consume LLFP, a preliminary study on the neutron-, proton-, deuteron-, and alpha particle-induced reaction cross sections at different incident energies was conducted. Figure 1 shows the cross-section data taken from TENDL-2015. The spallation cross sections of ^{90}Sr, ^{93}Zr, ^{107}Pd and ^{137}Cs are given in Fig. 1 as functions of incident energy ranging from 0 to 200 MeV, with comparisons of different incident particles, namely protons, deuterons, α particles, and neutrons.

Generally, the cross section increases with increasing energy and reaches a maximum at approximately 50 MeV, then decreases slowly. Over the main energy range studied, the cross sections of deuteron- or α particle-induced reactions are obviously larger than those of proton- or neutron-induced reactions at the same incident energy. The cross sections of protons and neutrons are approximately 1 b for ^{90}Sr, ^{93}Zr, and ^{107}Pd; however, the cross sections corresponding to the α particle and deuteron are distributed between 1.5 b and 2 b for these three isotopes. The cross sections of deuterons can reach 2.4 b for ^{137}Cs. There are no significant differences between the proton-induced reaction cross section and the neutron-induced reaction cross section. However, the cross sections corresponding to the α particle and deuteron are slightly different depending on the radionuclides.

Because the transmutation process is investigated to reduce the pollution and uncertainty occurring in conventional treatment methods, it is necessary to ensure that the transmutation products are less contaminating and less uncertain than the untreated LLFP [4]. Thus, all spallation products are divided into two categories, namely long-lived products and short-lived or stable products. An isotope is recognized as a long-lived product (or short-lived product) if its half-life is longer than one year (or shorter than one year). This criterion of one year is chosen because for an isotope with a half-life longer than one year, it takes more than ten years for it to completely (by 99.9% of the initial quantity) decay. The separated product cross sections of ^{90}Sr, ^{93}Zr, ^{107}Pd, and ^{137}Cs are shown in Fig. 2 as functions of incident energy ranging from 0-200 MeV, with comparisons of different incident particles, namely protons, deuterons, α particles, and neutrons.

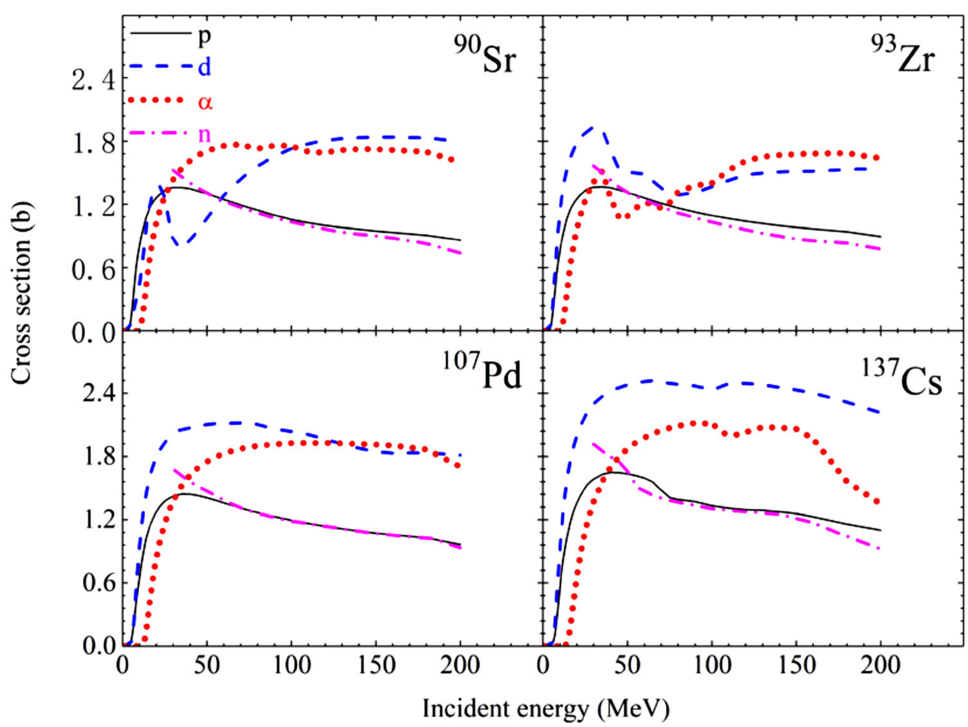

Fig. 1 (Color online) Total production cross sections of all spallation products heavier than the α particle for ^{90}Sr, ^{137}Cs, ^{107}Pd, and ^{93}Zr. The dot-dashed curves show the neutron-induced spallation reaction. The solid, dashed, and dotted curves show the spallation reactions induced by protons, deuterons, and α particles, respectively

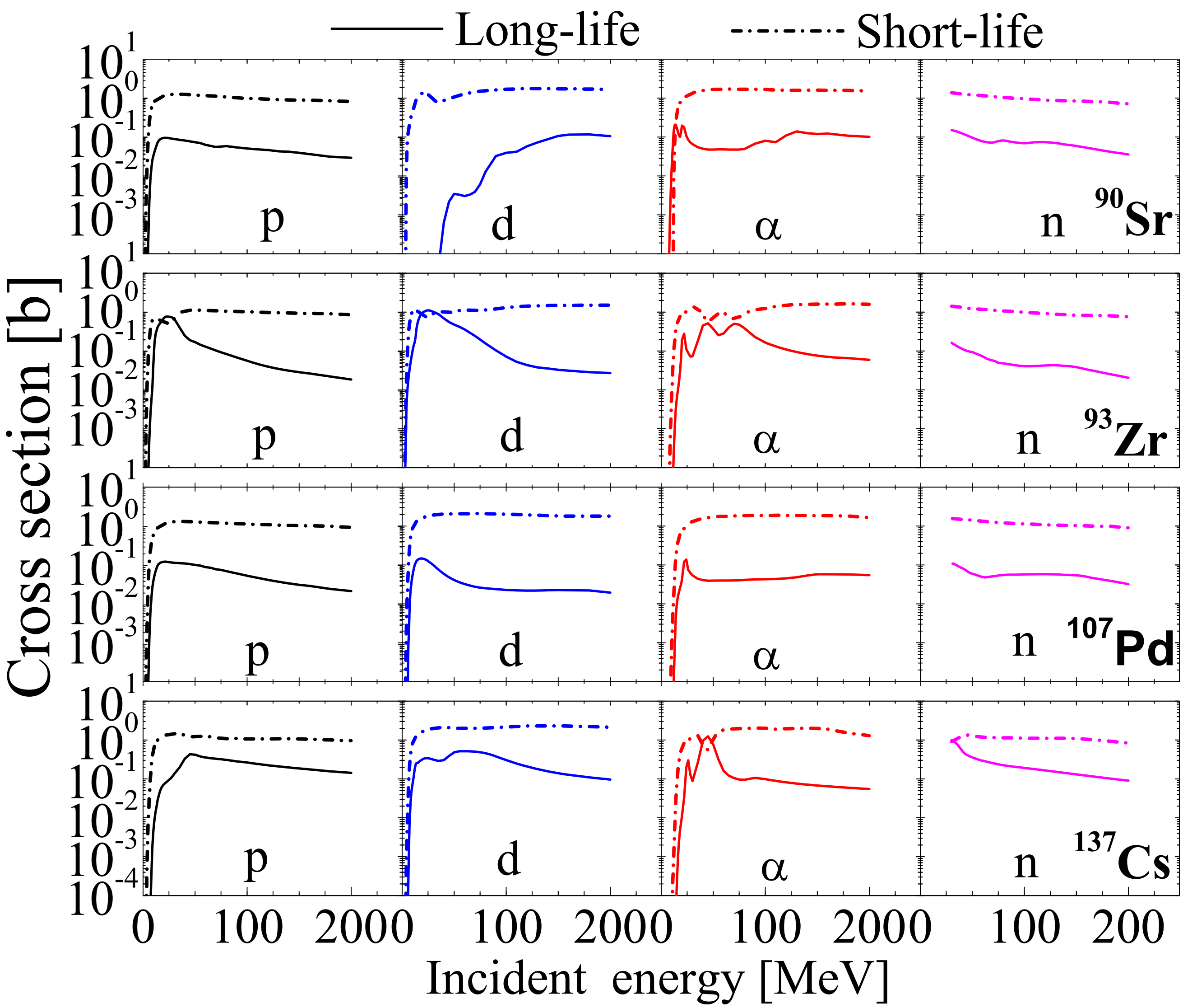

Fig. 2 (Color online) Production cross sections of long-lived spallation products and short-lived spallation products for ^{90}Sr, ^{137}Cs, ^{107}Pd, and ^{93}Zr. For each LLFP, the spallation products heavier than the α particle are divided into two categories, namely long-lived spallation products and short-lived spallation products, according to their half-lives. The former category is assigned to isotopes with a half-life longer than 1 year, labeled long-lived products. The latter is assigned to isotopes with a half-life of less than 1 year, labeled short-lived products. The dot-dashed curves show the neutron-induced spallation reaction. The solid, dashed, and dotted curves show the spallation reactions induced by protons, deuterons, and α particles, respectively

When the incident energy is higher than 100 MeV, for both long-lived products and short-lived products, the cross section is saturated, and the long-lived product cross sections are at least one order of magnitude lower than the short-lived product cross sections. For both ^{107}Pd and ^{90}Sr, the cross sections of the long-lived product are consistently less than 0.2 b in both the low-energy and high-energy regions, which are much smaller than those of short-lived products. This indicates that the resulting products are mostly short-lived or stable products when a thick ^{107}Pd target or ^{90}Sr target is bombarded by these light nuclei, regardless of the incident energy. For ^{137}Cs and ^{93}Zr, when the incident energy is lower than 100 MeV, the cross sections of the long-lived products are close to or even higher than those of the short-lived products. However, when the incident energy is higher than 100 MeV, the cross section corresponding to the long-lived nuclide in the product is less than 0.2 b. Therefore, we need to increase the incident energy to increase the relative production of short-lived isotopes in the product. Hence, based on the total production cross section and separated production cross section, the use of charged particle-induced spallation in LLFP transmutation is theoretically feasible.

3.2 Yield in transmutation

Because the light nuclide-induced reaction cross section depends largely on the incident energy, the energy loss of charged particles incident on a thick target needs to be considered, which is different from that in neutron-induced reactions. In the thick target model shown in Sect. 2, the specific energy loss S of charged particles in the absorber is fully considered, and the yield of the transmutation can be calculated using Eq. (5). As mentioned in the Method section, the electrons in the thick target can cause the velocity loss of incident charged particles by Coulomb force, and the velocity loss is more significant when the beam energy is low. Thus, it is necessary to enlarge the energy range to investigate the response of the transmutation system to incident high-energy particles. Because the total cross section does not vary significantly with the energy once the incident energy reaches 100 MeV for each curve presented in Sect. 3.1, it is reasonable to use the cross section at 200 MeV to replace the cross section of energy from 200 MeV to 1500 MeV.

Different spallation systems with targets made of one of the four isotopes, ^{90}Sr, ^{93}Zr, ^{107}Pd, and ^{137}Cs, are considered. For each system, the transmutation yield is calculated in the case of proton-, deuteron-, or α particle-induced reactions. Because neutrons are not charged, there is no velocity loss due to the stopping power of the target material. Once a neutron is incident in the thick target, it continues to travel through the target material and is reflected by the reflector covering the thick target until it reacts with a nuclide. Thus, the yield of transmutation using neutrons is approximately 1. The transmutation yields for different light nuclides and isotopes are shown in Fig. 3 as a function of incident energy ranging from 10 to 1500 MeV.

As shown in Fig. 3, the yield of transmutation using protons and the yield of transmutation using deuterons are much higher than that of using α particles at the same incident energy. When the incident energy is larger than 1000 MeV, the proton transmutation yield can almost reach 1, which is close to the yield of transmutation for neutrons. While the yield of transmutation using neutrons is higher than that for the three investigated charged particles at each incident energy, it is more expensive to obtain neutrons compared with charged particles of the same energy because of the difficulty of acceleration.

It was found that the yield of transmutation using protons or deuterons is more sensitive to energy changes when the incident energy is low and increase more slowly when the beam energy reaches 500 MeV. This can be explained by the more significant velocity loss of charged particles due to the Coulomb force and a smaller nuclear reaction cross section at low incident energy. The latter leads to a further reduction in the reaction cross section. At a high incident energy, the value of the reaction cross section is relatively large, and the velocity loss due to the Coulomb force is negligible compared to the initial speed. Hence, the incident particle continues to travel at the same speed and does not stop until it reacts with the target nucleus. Therefore, the yield of transmutation gradually increases and then reaches a maximum of approximately 1. Thus, it would not be an economical choice to transmute the investigated isotopes with incident energies higher than 500 MeV.

Because the common forms of LLFP are compounds rather than simple substances, the effects on the transmutation yield of LLFP due to the presence of other isotopes in the transmutation target were studied. Proton-induced transmutation systems with spallation targets made of Cs, CsF, and CsCl were considered. The transmutation cross sections for ^{137}Cs, ^{19}F, ^{35}Cl, and ^{37}Cl in proton-induced reactions are given as a function of incident energy ranging from 1 MeV to 200 MeV in Fig. 4.

It is shown in Fig. 4 that the total reaction cross sections in proton-induced spallation for ^{35}Cl, ^{37}Cl, and ^{19}F are of the same order of magnitude as that for ^{137}Cs in the studied energy range. Thus, the negative effects on the transmutation yield of LLFP due to the competition for incident protons between the ^{137}Cs nuclei and the chlorine (or fluorine) nuclei cannot be neglected. For the three target materials Cs, CsF, and CsCl, the transmutation yield of ^{137}Cs is given as a function of incident energy ranging from 10 MeV to 1500 MeV, as shown in Fig. 5.

The yield of transmutation using protons increases with increasing incident energy and remains stable when the incident energy reaches 1000 MeV. At the saturation stage, the yields of transmutation using protons are 0.9, 0.7, and 0.6 for ^{137}Cs, CsF, and CsCl, respectively. The transmutation yield of ^{137}Cs using protons is reduced by 1/4 for the spallation target made of CsF and 1/3 for that made of CsCl. At the same incident energy, the target materials corresponding to the absolute consumption from large to small are Cs, CsF, and CsCl. Despite the differences in values, similar shapes and trends are shared between the three curves. Thus, the light nuclide-induced reactions for elemental LLFP are considered to simplify the calculation in this study.

To gain a more intuitive understanding of the consumption of LLFP in light nuclide-induced transmutation, the consumption of each isotope within one year of the transmutation induced by protons at 500 MeV is calculated. It is assumed that the beam has a beam intensity of 5 mA, which is the highest beam intensity available with the China initiative accelerator-driven system. The masses of

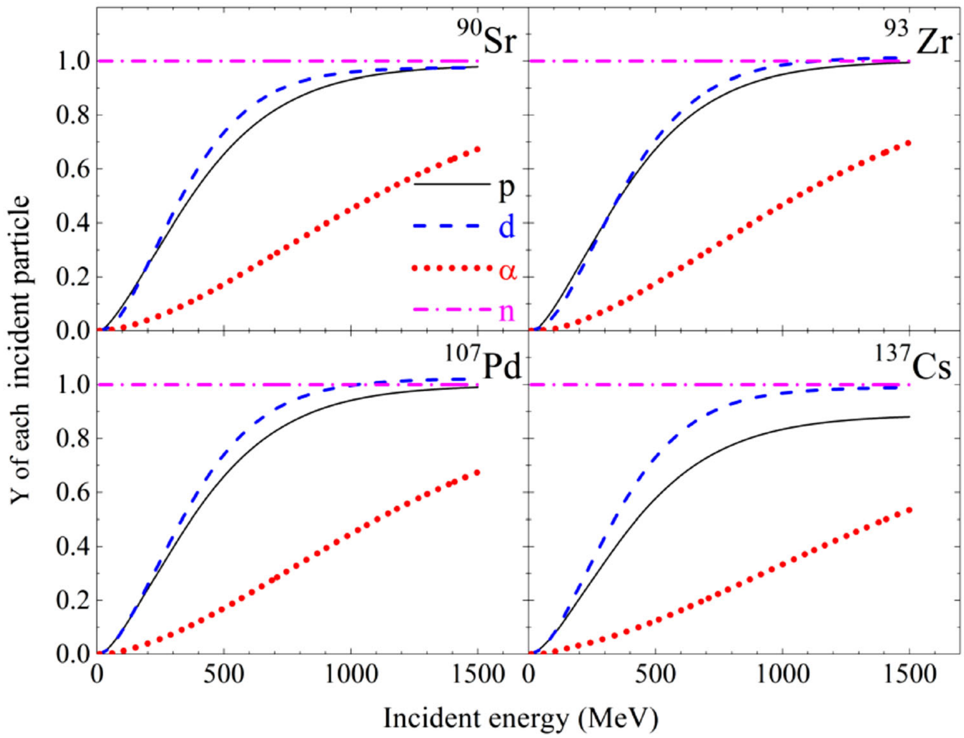

Fig. 3 (Color online) Transmutation yield of ^{90}Sr, ^{137}Cs, ^{107}Pd, and ^{93}Zr using spallation. The dot-dashed curves show the neutron-induced spallation reaction. The solid, dashed, and dotted curves show the spallation reactions induced by protons, deuterons, and α particles, respectively

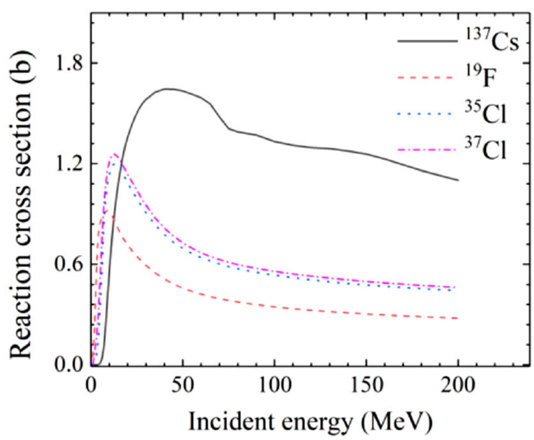

Fig. 4 (Color online) Total reaction cross section in proton-induced spallation for ^{137}Cs, ^{19}F, ^{35}Cl, and ^{37}Cl. The solid, dashed, dotted, and dot-dashed curves show the proton-induced spallation reactions of ^{137}Cs, ^{19}F, ^{35}Cl, and ^{37}Cl, respectively

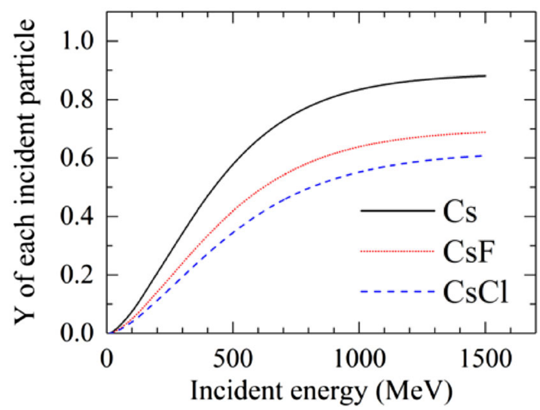

Fig. 5 (Color online) Yield of transmutation of ^{137}Cs using protons as a function of incident energy. The spallation targets consisting of elemental cesium and different cesium compounds are compared. The solid, dotted, and dashed curves show proton-induced spallation reactions with the targets consisting of elemental cesium, CsF, and CsCl, respectively

consumed isotopes are shown in Table 1, and the consumption of each isotope is approximately 100 g per year, which is not ideal compared with the amount of LLFP produced in nuclear reactors within one year. To make a prediction that is more accurate to the actual situation, the contribution of the secondary particles to the consumption of LLFP is considered in the last part of this section.

3.3 Contribution of secondary particles

Because a large number of neutrons, which can induce secondary reactions, are produced in the primary spallation reaction, it is considered that the neutrons, protons, deuterons, and α particles produced in the primary reaction can also contribute to the consumption of the target nuclei.

Based on the transmutation yields for each incident particle at different incident energies, the transmutation yield for each secondary particle can be calculated using

Table 1 Mass of ^{90}Sr, ^{137}Cs, ^{107}Pd, and ^{93}Zr transmuted by the primary and secondary particles within one year

LLFP	Consumption (g)	
	Primary particles	Primary and secondary particles
^{90}Sr	97.7	470.8
^{137}Cs	129.3	874.3
^{93}Zr	102.4	496.0
^{107}Pd	115.3	583.1

The transmutations are induced by protons at 500 MeV/nucleon with an intensity of 5 mA

the energy distribution of each light nuclide produced in the primary reaction. Taking neutrons as an example, the cross sections of neutrons produced in the p + ^{137}Cs reaction at 500 MeV/nucleon are given as a function of the produced neutron energy, as shown in Fig. 6. As shown in Fig. 6, the neutrons produced in the p + ^{137}Cs reaction at 500 MeV/nucleon have a distribution that is significantly concentrated in the energy range lower than 20 MeV. Moreover, it is shown in Fig. 1 that these neutrons with an emitted energy lower than 20 MeV have a larger cross section in the neutron-induced spallation of LLFP. Thus, compared with high-energy neutrons, secondary neutrons with an emitted energy lower than 20 MeV make a larger contribution to the transmutation yield of ^{137}Cs .

Because the transmutation yield of ^{137}Cs is calculated using the thick target model for neutrons at energies ranging from 0 to 1500 MeV, as shown in Fig. 3, the contribution of the secondary neutrons to the total transmutation yield of ^{137}Cs is calculated by summing up the transmutation yield of produced neutrons at different emitted energies.

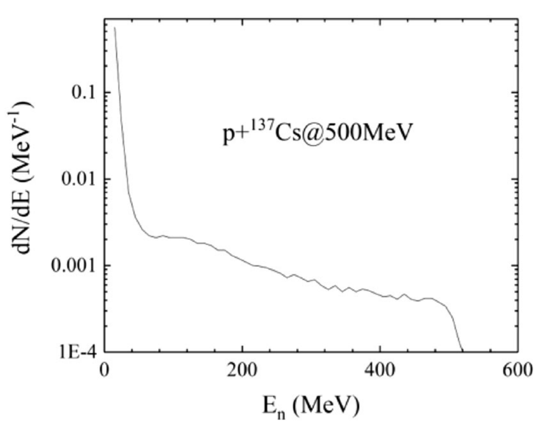

Fig. 6 Cross sections of neutrons produced in the p + ^{137}Cs reaction at 500 MeV/nucleon as a function of the produced neutron energy. The data are taken from Ref. [42]

For the economic reasons mentioned in Sect. 3.2, the proton-induced transmutation of ^{90}Sr, ^{93}Zr, ^{107}Pd, and ^{137}Cs at 500 MeV is considered. It is shown in the calculations that each secondary neutron can consume one target nuclide, each secondary proton can consume 0.15 to 0.2 target nuclei, each secondary deuteron can consume no more than 0.001 target nuclei, and each secondary α particle can consume no more than 1×10^{-6} target nuclei. Compared with the yield of transmutation for protons from the primary beam, the contribution of secondary neutrons and protons can increase the yield of transmutation by 300% and 20%, respectively. Figure 7 presents the transmutation yield for the primary protons, secondary neutrons, and secondary protons in the transmutation of ^{90}Sr, ^{93}Zr, ^{107}Pd and ^{137}Cs. It is shown in the figure that the transmutation yields for primary protons are between 0.5 and 0.7, the transmutation yields for secondary neutrons are between 2.3 and 3.2, and the transmutation yields for secondary protons are between 0.5 and 0.7. Because of the considerable contribution of the secondary particles, the total yield of transmutation using protons can reach 3 for ^{90}Sr, ^{93}Zr, and ^{107}Pd, and 4 for ^{137}Cs. Thus, the contribution of the secondary particles to the total consumption of target nuclei cannot be neglected compared with that of the primary beam.

The consumption of LLFP within one year is indicated by the total consumption of target nuclei by the reactions induced by both the primary beam and secondary particles. As in the calculation presented in Sect. 3.2, it is assumed that the transmutation is induced by protons at 500 MeV.

Based on the yield for each primary and secondary particle in the proton-induced transmutation of ^{90}Sr, ^{137}Cs, ^{107}Pd, and ^{93}Zr at 500 MeV/nucleon, the consumption of the same isotopes within one year of the transmutation induced by protons at 500 MeV was calculated. In addition,

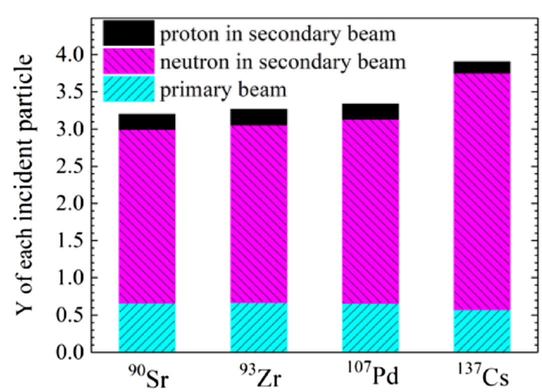

Fig. 7 (Color online) Transmutation yields for primary or secondary particles in the proton-induced transmutation of ^{90}Sr, ^{137}Cs, ^{107}Pd, and ^{93}Zr at 500 MeV/nucleon. The bottom, middle, and top of each bar shows the yield of each primary proton, secondary neutron, and secondary proton, respectively

it is assumed that a beam with an intensity of 5 mA is used, which is the highest beam intensity available with the China initiative accelerator-driven system. The masses of the consumed isotopesare listed as the last column in Table 1. It is shown that the total consumption of investigated isotopes can reach approximately 500 g per year, which is significantly higher than the mass of these isotopes consumed by the primary beam.

Furthermore, as shown in Fig. 3, the consumption of isotopes by per incident deuteron is slightly higher than that per incident proton. In addition, it is demonstrated in Ref. [42] that neutron cross sections in deuteron-induced spallation are higher than those in proton-induced spallation. Figure 7 shows that the total mass consumption is contributed mainly by secondary neutrons. Thus, it is reasonable to infer that the deuteron-induced transmutation can consume approximately 1 kg of LLFP with the particle beam accelerated by the China initiative accelerator-driven system.

4 Conclusion

In this study, the feasibility of transmuting LLFP ^{90}Sr, ^{93}Zr, ^{107}Pd, and ^{137}Cs induced by light nuclides, including neutrons, protons, deuterons, and α particles was investigated. The total production cross sections taken from TENDEL-2015 for each isotope in the spallation induced by different light nuclides at energies ranging from 10 to 200 MeV were compared. Over the main energy range studied, the cross sections of deuteron- or α particle-induced reactions are obviously larger than those induced by protons or neutrons at the same incident energy.

The spallation products were classified into long-lived and short-lived products according to their half-lives. When the incident energy is higher than 100 MeV, the short-lived product cross sections are one or two orders of magnitude larger than the long-lived product cross sections. This indicates that the use of charged particle-induced spallation in LLFP transmutation is theoretically feasible.

A thick target model was developed to calculate the yield of transmutation using different light nuclides in the transmutation of LLFP, in which the energy loss of incident charged particles due to charge interaction was considered. It was found that the yields of transmutation using protons and deuterons were much higher than that using α particles at the same incident energy. It is an economical choice to transmute these isotopes with an incident energy of 500 MeV. In addition, the transmutation yield was calculated for the proton-induced transmutation of ^{137}Cs in elemental and compound forms at 500 MeV. Because of the similarity between the yield of transmutation for elemental cesium and those for cesium compounds, the light nuclide-induced reactions for elemental LLFP were considered to simplify the calculation.

The yields of transmutation for each primary or secondary particle in proton-induced transmutation of ^{90}Sr, ^{93}Zr, ^{107}Pd, and ^{137}Cs at 500 MeV/nucleon were calculated. It was found that the contribution of secondary neutrons and protons can increase the yield of transmutation using protons by 300% and 20%, respectively, compared with the yield of each proton from the primary beam.

Under the irradiation of a proton beam with a beam intensity of 5 mA, which is the highest beam intensity provided by the China initiative accelerator-driven system, the consumption of four LLFP can reach 500 grams per year when both the primary beam and the secondary particles are considered.

Exceedingly ideal assumptions were made in the calculations. For example, a target with an infinitely large surface is considered to prevent the incident beam from escaping; a target made of elemental LLFP rather than compounds is considered as well. These assumptions are difficult to realize in practical applications. Nevertheless, the upper limit of transmutation consumption is given by the calculations. This value (approximately 500 g/year) suggests the possibility of transmuting LLFP with spallation, though its economics and feasibility are still far below the achievable range. Further research on improving the beam intensity is required in the future.

Author Contributions All authors contributed to the study conception and design. Material preparation, data collection and analysis were performed by Meng-Ting Jin, Su-Yang Xu, Guan-Ming Yang, and Jun Su. The first draft of the manuscript was written by Meng-Ting Jin and all authors commented on previous versions of the manuscript. All authors read and approved the final manuscript.

References

1. V.M. Efremenkov, Radioactive waste management at nuclear power plants. Int. Atom. Energy Agency Bull. **31**, 37–42 (1989)
2. P.A. Kharecha, J.E. Hansen, Prevented mortality and greenhouse gas emissions from historical and projected nuclear power. Environ. Sci. Technol. **47**, 4889–4895 (2013). https://doi.org/10.1021/es3051197
3. R.E. Sims, H.H. Rogner, K. Gregory, Carbon emission and mitigation cost comparisons between fossil fuel, nuclear and renewable energy resources for electricity generation. Energy Policy **31**, 1315–1326 (2003). https://doi.org/10.1016/S0301-4215(02)00192-1
4. A.C. Mueller, Nuclear waste incineration and accelerator aspects from the european pds-xads study. Nuclear Phys. A **751**, 453–468 (2005). In: Proceedings of the 22nd International Nuclear Physics Conference (Part 1). https://doi.org/10.1016/j.nuclphysa.2005.02.015

5. J. Schapira, Gedeon: A joint venture between research (cea and cnrs) and industry (edf and framatome). Nuclear Phys. A **654**, C458–C466 (1999). In: Proceedings of the International Nuclear Physics Conference. https://doi.org/10.1016/S0375-9474(99)00270-5
6. B.K. Sovacool, A critical evaluation of nuclear power and renewable electricity in Asia. J. Contemp. Asia **40**, 369–400 (2010). https://doi.org/10.1080/00472331003798350
7. A. Olacel, C. Borcea, P. Dessagne et al., Neutron inelastic cross-section measurements for ^{24}Mg. Phys. Rev. C **90**, 034603 (2014). https://doi.org/10.1103/PhysRevC.90.034603
8. M. Salvatores, I. Slessarev, A. Tchistiakov, The transmutation of long-lived fission products by neutron irradiation. Nucl. Sci. Eng. **130**, 309–319 (1998). https://doi.org/10.13182/NSE98-A2008
9. C. Paradela, L. Tassan-Got, L. Audouin et al., Neutron-induced fission cross section of ^{234}U and ^{237}Np measured at the cern neutron time-of-flight (n_tof) facility. Phys. Rev. C **82**, 034601 (2021). https://doi.org/10.1103/PhysRevC.82.034601
10. W. Gudowski, Accelerator-driven transmutation projects. the importance of nuclear physics research for waste transmutation. Nuclear Phys. A **654**, C436–C457 (1999). In: Proceedings of the International Nuclear Physics Conference. https://doi.org/10.1016/S0375-9474(99)00269-9
11. K. Fraval, F. Gunsing, S. Altstadt et al., Measurement and analysis of the ^{241}Am(n,γ) cross section with liquid scintillator detectors using time-of-flight spectroscopy at the n_tof facility at cern. Phys. Rev. C **89**, 044609 (2014). https://doi.org/10.1103/PhysRevC.89.044609
12. IAEA, Implications of Partitioning and Transmutation in Radioactive Waste Management, Technical Reports Series No. 435, IAEA, Vienna (2004)
13. W. Wlazło, T. Enqvist, P. Armbruster et al., Cross sections of spallation residues produced in 1*A* GeV ^{208}Pb on proton reactions. Phys. Rev. Lett. **84**, 5736–5739 (2000). https://doi.org/10.1103/PhysRevLett.84.5736
14. T. Enqvist, P. Armbruster, J. Benlliure et al., Primary-residue production cross sections and kinetic energies in 1*A* GeV ^{208}Pb on deuteron reactions. Nucl. Phys. A **703**, 435–465 (2002). https://doi.org/10.1016/S0375-9474(01)01340-9
15. H.Y. Meng, Y.W. Yang, Z.L. Zhao et al., Physical studies of minor actinide transmutation in the accelerator-driven subcritical system. Nucl. Sci. Tech. **30**, 91 (2019). https://doi.org/10.1007/s41365-019-0623-1
16. Z.L. Zhao, Y.W. Yang, S. Hong, Application of fluka and openmc in coupled physics calculation of target and subcritical reactor for ads. Nucl. Sci. Tech. **30**, 10 (2019). https://doi.org/10.1007/s41365-018-0539-1
17. H. Wang, H. Otsu, H. Sakurai et al., Spallation reaction study for fission products in nuclear waste: cross section measurements for ^{137}Cs and ^{90}Sr on proton and deuteron. Phys. Lett. B **754**, 104–108 (2016). https://doi.org/10.1016/j.physletb.2015.12.078
18. V. Artisyuk, M. Saito, A. Stankovsky, Challenge of transmutation of long-lived nuclides. Prog. Nucl. Energ. **47**, 327–338 (2005). https://doi.org/10.1016/j.pnucene.2005.05.031
19. H. Yapıcı, N. Demir, G. Genç, Neutronic analysis for transmutation of minor actinides and long-lived fission products in a fusion-driven transmuter (fdt). J. Fusion Energy **25**, 225–239 (2006). https://doi.org/10.1007/s10894-006-9027-4
20. H. Yapıcı, G. Genç, N. Demir, A comprehensive study on neutronics of a lead-bismuth eutectic cooled accelerator-driven sub-critical system for long-lived fission product transmutation. Ann. Nucl. Energ. **35**, 1264–1273 (2008). https://doi.org/10.1016/j.anucene.2007.12.007
21. Z.X. Fang, M. Yu, Y.G. Huang et al., Theoretical analysis of long-lived radioactive waste in pressurized water reactor. Nucl. Sci. Tech. **32**, 72 (2021). https://doi.org/10.1007/s41365-021-00911-0
22. J.Y. Tang, Q. An, J.B. Bai et al., Back-n white neutron source at csns and its applications. Nucl. Sci. Tech. **32**, 11 (2021). https://doi.org/10.1007/s41365-021-00846-6
23. R. Xu, Z.J. Wang, Y.Y. Xue et al., Displacement damage in optocouplers induced by high energy neutrons at back-n in china spallation neutron source. Chin. Phys. B **29**, 014210 (2020). https://doi.org/10.1088/1674-1056/ab5efb
24. Y. Liu, W. Chen, C. He et al., Analysis of displacement damage effects on bipolar transistors irradiated by spallation neutrons. Chin. Phys. B **28**, 067302 (2019). https://doi.org/10.1088/1674-1056/28/6/067302
25. T. Hayakawa, S. Miyamoto, R. Hajima et al., Proposal for selective isotope transmutation of long-lived fission products using quasi-monochromatic γ -ray beams. J. Nucl. Sci. Technol. **53**, 2064–2071 (2016). https://doi.org/10.1080/00223131.2016.1194776
26. R. Nagai, R. Hajima, M. Mori, et al., Demonstration of high-flux photon generation from an erl-based laser compton photon source. TUPJE002, these proceedings, IPAC **15**. https://doi.org/10.18429/JACoW-IPAC2015-TUPJE002
27. D. Li, K. Imasaki, K. Horikawa et al., Iodine transmutation through laser compton scattering gamma rays. J. Nucl. Sci. Technol. **46**, 831–835 (2009). https://doi.org/10.1080/18811248.2007.9711592
28. H. Ejiri, T. Shima, S. Miyamoto et al., Resonant photonuclear reactions for isotope transmutation. J. Phys. Soc. Japan **80**, 094202 (2011). https://doi.org/10.1143/JPSJ.80.094202
29. H. Harada, T. Baba, M. IgasFFira et al., Plan of LLFP neutron cross section measurements for nuclear transmutation. J. Nucl. Sci. Technol. **39**, 366–368 (2002). https://doi.org/10.1080/00223131.2002.10875116
30. A. Hermanne, Transmutation of long lived fission products: the possibilities of proton induced reactions. J. Nucl. Sci. Technol. **39**, 1202–1205 (2002). https://doi.org/10.1080/00223131.2002.10875318
31. H. Wada, S. Nakamura, K. Furutaka et al., Production of the isomeric state of ^{138}Cs in the thermal neutron capture reaction ^{137}Cs (n, γ) ^{138}Cs . J. Nucl. Sci. Technol. **37**, 827–831 (2000). https://doi.org/10.1080/18811248.2000.9714963
32. S. Nakamura, K. Furutaka, H. Wada et al., Measurement of the thermal neutron capture cross section and the resonance integral of the $^{90}extSr$ (n, *gamma*) $^{91}extSr$ reaction. reaction. J. Nucl. Sci. Technol. **38**, 1029–1034 (2001). https://doi.org/10.1080/18811248.2001.9715132
33. S. Kunieda, N. Furutachi, F. Minato et al., JENDL/ImPACT - 2018: a new nuclear data library for innovative studies on transmutation of long-lived fission products. J. Nucl. Sci. Technol. **56**, 1073–1091 (2019). https://doi.org/10.1080/00223131.2019.1647889
34. C.W. Ma, D. Peng, H.L. Wei et al., Isotopic cross-sections in proton induced spallation reactions based on the bayesian neural network method. Chin. Phys. C **44**, 014104 (2020). https://doi.org/10.1088/1674-1137/44/1/014104
35. G. Yang, S. Xu, M. Jin et al., Prediction of the cross-sections of isotopes produced in deuteron-induced spallation of long-lived fission products. Chin. Phys. C **43**, 104101 (2019). https://doi.org/10.1088/1674-1137/43/10/104101
36. W. Sun, W. Qiu, J. Su, Production of high-energy neutrons by interaction of a deuteron beam with matter. Appl. Radiat. Isotop. **174**, 109752 (2021). https://doi.org/10.1016/j.apradiso.2021.109752

37. Q.F. Song, S.Y. Xu, J. Su, Nucleon stripping in deuteron-induced spallation reactions at hundreds mev/nucleon. Chin. Phys. C **45**, 044101 (2021). https://doi.org/10.1088/1674-1137/abde31
38. Z. Wang, F. Wang, G. Huang, in 10th Int. Particle Accelerator Conf. (IPAC'19), Melbourne, Australia, 19–24, et al., The status of ciads superconducting linac. JACOW Publishing, Geneva, Switzerland **2019**, 994–997 (2019)
39. Y. Qin, P. Zhang, H. Cai et al., Transfer line including vacuum differential system for a high-power windowless target. Phys. Rev. Accel. Beams **23**, 113002 (2020). https://doi.org/10.1103/PhysRevAccelBeams.23.113002
40. P. Sigmund, Particle penetration and radiation effects springer series in solid-state physics. (2006)
41. G.F. Knoll, *Radiation Detection and Measurement* (Wiley, 2010)
42. S. Xu, G. Yang, M. Jin et al., Probing the deuteron breakup and linking the cross sections of residue production between the neutron- and deuteron-induced spallation at 500 MeV/nucleon. Phys. Rev. C **101**, 024609 (2020). https://doi.org/10.1103/PhysRevC.101.024609